ELSEVIER

Nuclear Physics A 592 (1995) 291–306

NUCLEAR PHYSICS A

Chaotic dynamics of single particles in axially symmetric nuclear shapes

Tapan Mukhopadhyay, Santanu Pal

Variable Energy Cyclotron Centre, 1/AF Bidhan Nagar, Calcutta 700 064, India

Received 29 September 1994; revised 11 April 1995

Abstract

The spectral statistics of single particle motion in deformed cavities with axial symmetry are presented. Considering cavities with Legendre-polynomial deformations P_2 to P_6, a systematic study of the fluctuation measures of the energy spectra is performed. For each deformation type, the evolution of the fluctuation measures with increasing deformation indicating an order-to-chaos transition is observed. The nature of such transitions is found to be in agreement with earlier classical phase space calculations.

1. Introduction

The study of chaotic dynamics in hamiltonian systems has become one of the fastest growing disciplines during the recent years. Although one would naturally expect a chaotic dynamics in complex systems, the main interest in such studies stems from the fact that chaos is found [1] to be present in the dynamics of even simple systems with a few degrees of motion. In spite of being a many-body complex system, the atomic nucleus also exhibits features which are typical of motions involving relatively fewer degrees of freedom, such as single particle and collective motions. This makes the nucleus an interesting system to look for chaotic dynamics in these degrees of freedom. In particular, it is of interest to study the nature of single particle motion in nuclei with large deformations, since mean field dynamics is found [2] to be valid even for super- and hyperdeformed nuclear shapes.

Arvieu et al. [3] considered the classical motion of a particle moving in a deformed potential and pointed out the importance of the topology of phase space to characterise such motions. The order-to-chaos transition in the classical dynamics of a particle in various Legendre-deformed (P_2 to P_6) cavities were subsequently studied [4,5]

SSDI 0375-9474(95)00312-6

employing Poincaré sections. It was further concluded in Ref. [4] from a study of cavities with oscillating walls that the nucleus responds either as an elastic solid or as a viscous fluid depending upon the two limiting conditions of a fully regular or a fully chaotic single particle motion. The importance of octupole deformation in the presence of a quadrupole deformation in establishing chaotic single particle motion was demonstrated by Heiss et al. [6].

In a recent investigation of the motion of the nucleons in a deformed potential, Bauer et al. [7] however observed that the collective motion is not damped even when the single particle dynamics is a chaotic one. A crucial ingredient in this calculation was the inclusion of self-consistency in the oscillating part of the mean field potential. This raises the important question of the role of self-consistency in the dissipative dynamics of collective motion of finite Fermi systems. It may be pointed out at this stage, however, that only mild chaos was considered in Ref. [7] compared to those considered by Blocki et al. [4,5]. The largest Lyapunov exponent obtained in the self-consistent calculation [7] is 2×10^{-3} whereas it is much larger than 10^{-2} for all the non-integrable cases considered in Refs. [4,5]. In fact, it was shown in Ref. [4] that the dynamics is mostly conservative for a particle in a cavity undergoing shape oscillations without self-consistency for a weakly chaotic single particle motion. We, therefore, feel that further investigations are required considering non-integrable self-consistent systems with strong chaos in the microscopic dynamics before we draw any conclusion on the role of self-consistency in the dissipative dynamics of the macroscopic motion.

In the present paper, we shall concern ourselves with the chaotic features in the quantum mechanical description of a particle in a deformed potential. Although a precise definition of chaos in quantum systems is still lacking, semiclassical methods have been successful in showing that the fluctuations in the density of the quantal energy eigenvalues fall into universality classes determined essentially by the nature of the underlying classical dynamics. Among the typical fluctuation measures commonly used are the nearest neighbor level-spacing distribution $P(s)$ and the spectral rigidity Δ_3. Their behavior is quite distinct for the two extreme cases of either a fully regular or a fully chaotic dynamics in the corresponding classical systems. In the generic case, where the phase space is mixed, the statistics is intermediate.

The plan of the present paper is as follows. Firstly, we study how well the fluctuation measures reflect the non-integrability of deformed cavities. To this end, we calculate the single particle energy spectrum in axially symmetric deformed non-integrable cavities with Legendre polynomial deformations P_2 through P_6 and obtain the systematics of the fluctuation measures. Subsequently we find the degree of chaos in the single particle dynamics in deformed cavities which are typically found in the shape oscillations of the giant resonances in nuclei. Since in a macroscopic picture [8] the isoscalar giant multipole resonances can be considered as incompressible shape oscillations and the coupling of this shape oscillation with the single particle motion of the nucleons is considered to be one of the important mechanisms for the damping of the resonances, it is imperative to know the nature of the single particle motion because, as mentioned earlier, a chaotic single particle motion is expected to lead to a damping of the collective

motion. This, in fact, is the main motivation of the present work.

In the next section, we describe the model and briefly sketch the essential steps to calculate the eigenenergies in a deformed cavity. Systematics of the fluctuation properties analyzed in Section 3. Finally, Section 4 contains a summary and discussions of our results.

2. Single particle dynamics in a deformed cavity

In the extreme single particle description of a nucleus, the nucleons move independently in an average uniform leptodermous potential. For the sake of simplicity, we shall take a cavity for this potential which rises steeply to infinity at the surface. We shall consider only axially symmetric systems whose surface will be deformed according to Legendre polynomials of different orders,

$$R(\theta) = \frac{R_0}{\lambda}[1 + \alpha_n P_n(\cos\theta)], \tag{2.1}$$

where R_0 is the radius of a sphere having the same volume as the deformed cavity, λ is a volume preserving factor and α_n is the strength of the deformation. The Schrödinger equation for a particle of mass M and energy E inside the cavity will be

$$\nabla^2\psi = k^2\psi \text{ for } r < R(\theta), \tag{2.2}$$

where $k = (2ME/\hbar^2)^{1/2}$.

To obtain the eigenenergies of Eq. (2.2), we proceed as follows. Making the expansion

$$\psi_m(r,\theta,\phi) = \sum_l a_l j_l(kr) P_l^m(\cos\theta)\exp(im\phi), \tag{2.3}$$

where m is the azimuthal quantum number, and imposing the boundary condition $\psi_m(R(\theta)) = 0$ on the surface, we get the following set of simultaneous equations:

$$\sum_l a_l B_{l'l}(k) = 0, \tag{2.4}$$

where

$$B_{l'l}(k) = \int_0^\pi P_{l'}^m(\cos\theta) j_l(kR(\theta)) P_l^m(\cos\theta) d(\cos\theta).$$

The energy eigenvalues are determined by requiring that the determinant of the matrix $B(k)$ vanish, i.e. an eigenvalue corresponds to that value of k for which $\det[B(k)]$ is zero. In principle, the matrix B is infinite dimensional. In a numerical calculation, B is truncated while ensuring that the energy eigenvalues are stable. For each deformation, a large number of eigenvalues (typically 500) are numerically obtained for a given parity and azimuthal quantum number. Each sequence of levels is then unfolded to give a mean density of unity. The unfolded levels are denoted by ϵ_n and will be used in the next section for evaluating the spectral distributions.

3. Fluctuation properties of the energy spectrum

The nearest neighbor level-spacing distribution (NNLD), $P(s)$, is defined such that it is the probability of finding pairs $(\epsilon_i, \epsilon_{i+1})$ with spacing between s and $s+ds$. Since the normal histogram representation depends sensitively on the bin size, we expand $P(s)$ in terms of Laguerre polynomials $L_n(s)$ [9],

$$P(s) = \frac{1}{N}\sum_{i=1}^{N}\delta(s - s_i) = \sum_n C_n L_n(s)\exp(-s)\,, \tag{3.1}$$

where $N+1$ is the total number of levels and C_n's are the coefficients to be determined. Convergence is numerically found to be excellent with a 20-term expansion.

For generic integrable systems, $P(s)$ is the Poisson distribution $\exp(-s)$, indicating a clustering of levels. This result is based on the semi-classical periodic orbit theory [10]. For chaotic systems with time-reversal invariance, numerical explorations on a number of systems [11] show that $P(s)$ is well approximated by the Wigner distribution,

$$P(s) = \frac{\pi}{2} s\, e^{-\pi s^2/4}\,, \tag{3.2}$$

which is close to the fluctuations of the eigenvalues of Gaussian Orthogonal Ensembles (GOE) of random matrices with antiunitary symmetry. This distribution characterizes a repulsion between neighboring levels in sharp contrast to the clustering observed for integrable systems.

The spectral rigidity Δ_3 is the first measure for which expressions have been obtained using the periodic orbit theory for both integrable and chaotic cases [12]. It is defined as

$$\Delta_3(L) = \left\langle \min_{a,b} \frac{1}{L}\int_{-L/2}^{+L/2} [N(x+\epsilon) - a - b\epsilon]^2 d\epsilon \right\rangle \tag{3.3}$$

and is a measure of the average least-square deviation of the spectral staircase of the unfolded spectra (mean spacing unity), $N(\epsilon)$, from the best fitting straight line $a+b\epsilon$. In the above equation, $\langle\ \rangle$ denotes local averaging around x. The semiclassical density of states in terms of classical periodic orbits:

$$d(E) = d_{av}(E) + \frac{1}{\hbar^{\nu+1}}\sum_j A_j(E) e^{iS_j(E)/\hbar} \tag{3.4}$$

can be used to express the spectral rigidity [14] as

$$\Delta_3(L) = \frac{2}{\hbar^{2\nu}}\int_0^{\infty} \frac{dT}{T^2}\phi(T) G\left(\frac{LT}{2\hbar}\right)\,, \tag{3.5}$$

where $G(y) = 1 - F^2(y) - 3F'^2(y)$, $F(y) = \sin(y)/y$ and ν takes values, 0 or $(N-1)/2$ depending on whether the system is chaotic or regular, N being the number of degrees

of freedom. In Eq. (3.4), j is the label for all distinct classical periodic orbits. The form factor

$$\phi(T) = \langle \sum_i \sum_j A_i A_j \cos[(S_i - S_j)/\hbar] \delta_{ij}(T - \frac{T_i + T_J}{2}) \rangle \tag{3.6}$$

is crucial in the analysis and embodies the collective properties of the periodic orbits. Here S_i and T_i refer to the reduced action and time period of the orbit and A_i is the amplitude that occurs in Eq. (3.4) above. For the integrable and chaotic cases, $\phi(T)$ has distinct universality classes [12,13] which manifest directly in $\Delta_3(L)$ for values of $L \ll L_{\max}$ where $L_{\max}$ is given as [12],

$$L_{\max} = h\langle d \rangle / T_{\min} \tag{3.7}$$

where $\langle d \rangle$ is the average level density and $T_{\min}$ is the period of the shortest classical closed orbit. Thus

$$\begin{aligned} \Delta_3 &= L/15, \quad \text{for integrable and} \\ &= \ln(L)/\pi^2 - 0.00695, \quad \text{when chaotic with time reversal.} \end{aligned} \tag{3.8}$$

For large L, the behaviour of $\Delta_3(L)$ depends on the orbit selection function, $G(y)$ which saturates for $y > \pi$. Thus for $L \gg L_{\max}$, the contribution of even the shortest orbit ceases to vary as a function of L and this leads to a saturation in the spectral rigidity.

3.1. Variation of $P(s)$ and Δ_3 with deformation

Here we shall study the variation of the nearest neighbor level-spacing distribution, $P(s)$ and the spectral rigidity Δ_3 with the cavity deformation. For a cavity with quadrupole deformation, Fig. 1 shows the variation of the $P(s)$ and Δ_3 distributions with the deformation parameter α_2, which is changed from zero (spherical) to positive values (prolate). The level sequences considered are for azimuthal quantum number $m = 0$ states and are of even parity. The $P(s)$ distribution for the integrable spherical cavity is very close to an ideal Poisson distribution, as expected. As the cavity is progressively deformed making the system non-integrable, the NNLD changes towards the GOE distribution. However, the GOE limit is not fully attained even at the largest deformation ($\alpha_2 = 0.4$) shown here. For smaller deformations, the $P(s)$ distributions are intermediate between the two ideal distributions, Poisson and GOE, and can be associated with a partially chaotic motion. Similar order-to-chaos transitions were also observed [4] for the motion of classical particles in deformed cavities.

The spectral rigidity Δ_3 in Fig. 1 shows the universal nature of the distribution for $L \ll L_{\max}$. The positions of $L_{\max}$ are also shown in this figure. As expected, Δ_3 of the spherical cavity is close to $L/15$, an ideal Poisson distribution, for $L \ll L_{\max}$. Subsequently the spectral rigidity moves towards the GOE limit with increasing deformation. However, the full GOE limit is not attained for the cases considered here which is also similar

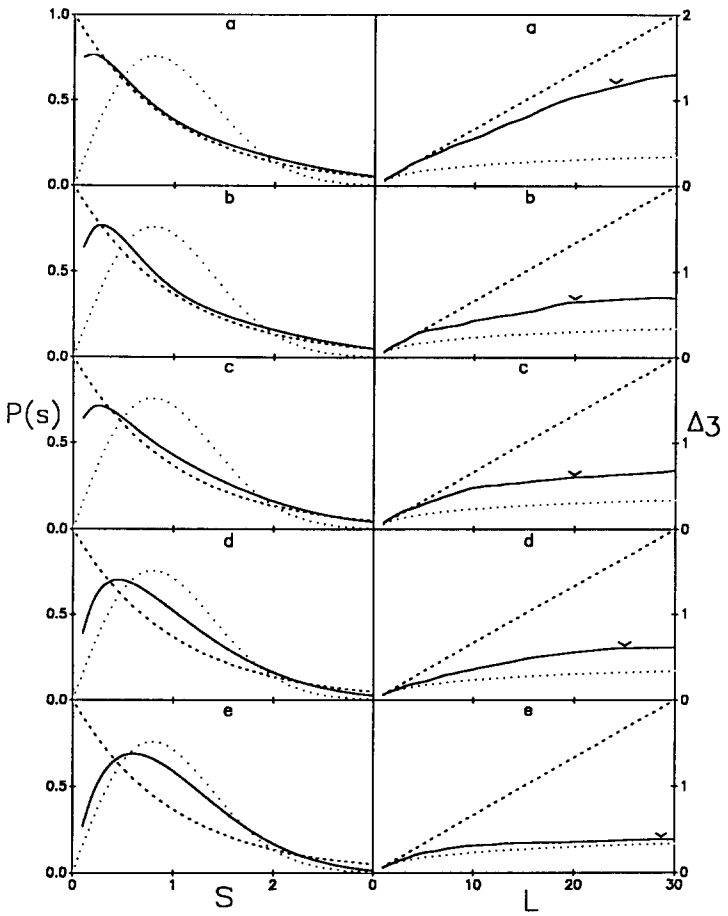

Fig. 1. The nearest neighbor level-spacing distribution $P(s)$ and the spectral rigidity Δ_3 in a cavity with quadrupole deformation for increasing values of the deformation parameter α_2 starting from the top. The solid lines are the calculated distributions. The ideal Poisson (dashed line) and ideal Wigner (dotted line) distributions are also shown. The figures marked (a), (b), (c), (d) and (e) are for $\alpha_2 = 0.0$, 0.05, 0.1, 0.2 and 0.4, respectively. The level sequences are of $m = 0$ and even parity states. In Δ_3 distributions, the positions of L_{max} are shown as marked (∨).

to the nature of the $P(s)$ distribution. For L values close to L_{max}, both short and long periodic orbits contribute to the spectral rigidity (Eq. (3.6)) and their interplay makes the Δ_3 distribution to deviate from the universal values. It is further evident that the non-universal domain of $L \gg L_{max}$ is beyond the range of the plots in this figure. This, however, is of little consequence for the present study where we concentrate upon the evolution of the Δ_3 distribution with deformation in the universal region.

The spectral statistics of the odd parity states for the same systems are shown in Fig. 2. Both the $P(s)$ and Δ_3 distributions are very similar to those of the positive parity states showing regular to chaos transition with increasing deformation. It is of interest to note here that though the eigenfunctions of the positive and negative parity states have very

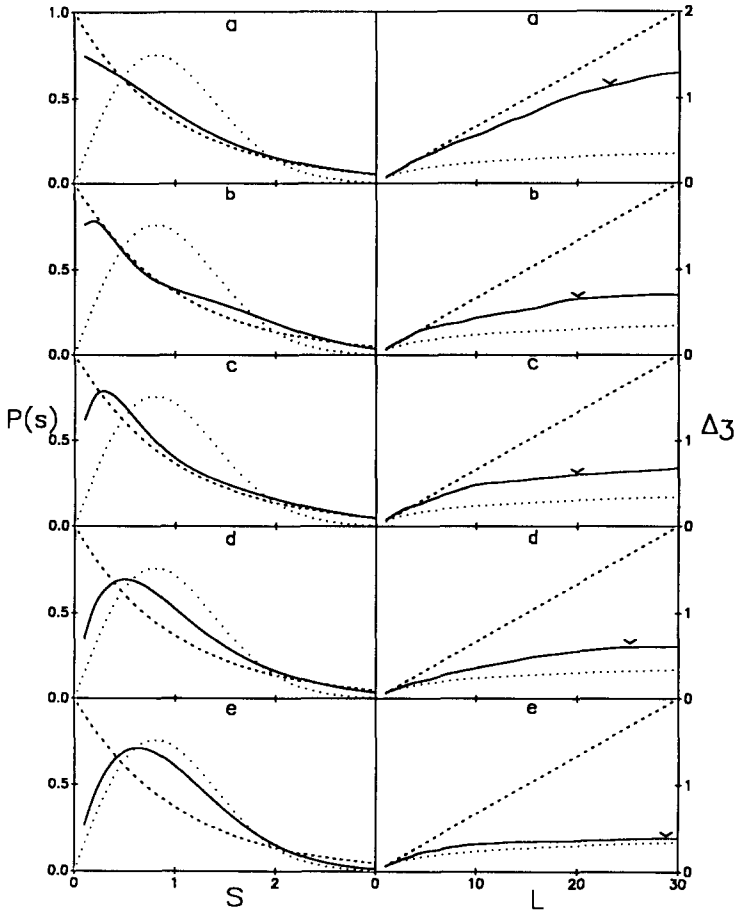

Fig. 2. Same as Fig. 1, but for odd parity states.

different nodal structures, their eigenenergies possess very similar fluctuation measures both being governed by the same underlying classical motion.

We next considered the systematics of the spectral fluctuations as the cavity is deformed to oblate shapes. Fig. 3 shows the $P(s)$ and Δ_3 variations with α_2, now assuming negative values, for even parity states. We find that the distributions change in a similar manner as in Fig. 1. However, both the $P(s)$ and Δ_3 for oblate cavities are closer to the GOE compared to the prolate cases at large deformations, i.e. $|\alpha_2| > 0.2$. This possibly reflects the fact that for the same $|\alpha_2|$, the asymmetry of the cavity defined as the ratio of the major to the minor axis, is higher for an oblate shape than for a prolate one and the asymmetry increases faster with increasing $|\alpha_2|$ for oblate deformations. We also made similar observation for the systematics of the odd parity states.

One of the interesting results from the studies [4,5] of the classical phase space of single particle dynamics in axially symmetric potentials is that the trajectories with higher angular momentum component (m) along the symmetry axis are less chaotic.

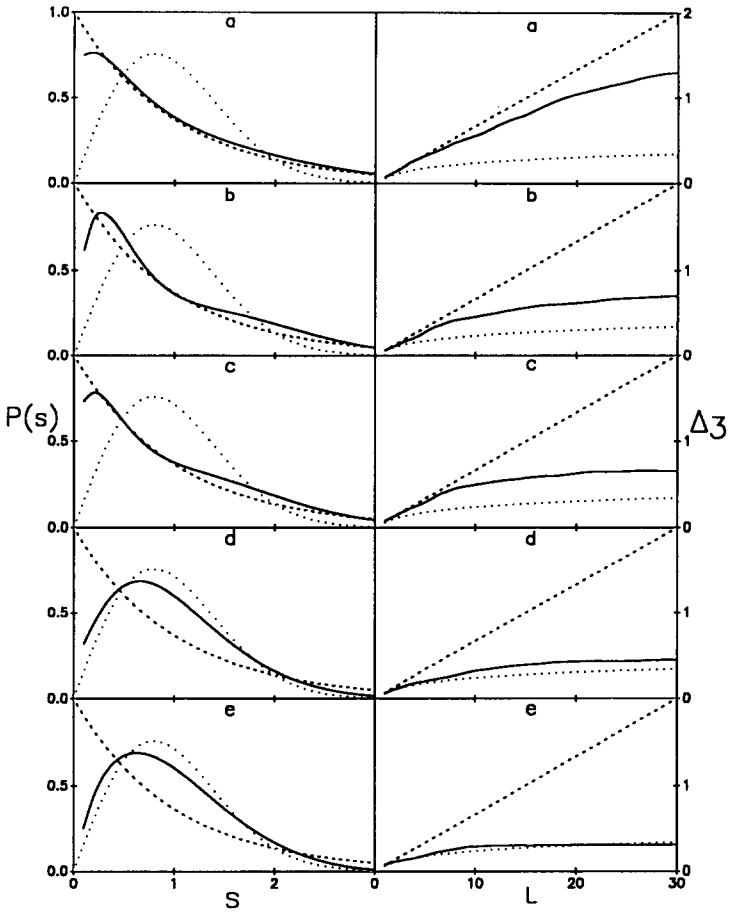

Fig. 3. Same as Fig. 1, but for negative values of the deformation parameter α_2. The figures marked (a), (b), (c), (d) and (e) are for $\alpha_2 = 0.0$, -0.05, -0.1, -0.2 and -0.4, respectively. The level sequences are of $m = 0$ and even parity states.

To see if this is reflected in the statistics of quantum energy spectrum, we calculated the $P(s)$ and Δ_3 distributions for an eigenvalue sequence with $m = 6$ and Fig. 4 shows the comparison with the $m = 0$ distributions. Indeed, we find that both the $P(s)$ and Δ_3 distributions for the $m = 6$ levels are closer to the ideal Poisson distributions than the $m = 0$ case. This corroborates the classical observation [4] that the centrifugal force confines the higher m trajectories near the equatorial zone whereas the lower m trajectories can go anywhere. Since the variation of the curvature of the potential is slower near the equator, the dynamics of the higher m states are more regular.

The value of each L_{max} shown in the figures for P_2 deformed cavities is obtained from Eq. (3.7) using $\langle d \rangle$ from the calculated spectra and T_{min} from the length of the shortest periodic orbit (along the semi-minor axis) divided by the speed at the centroid of the averaging energy interval. However, the nature of the periodic orbits in the cavities

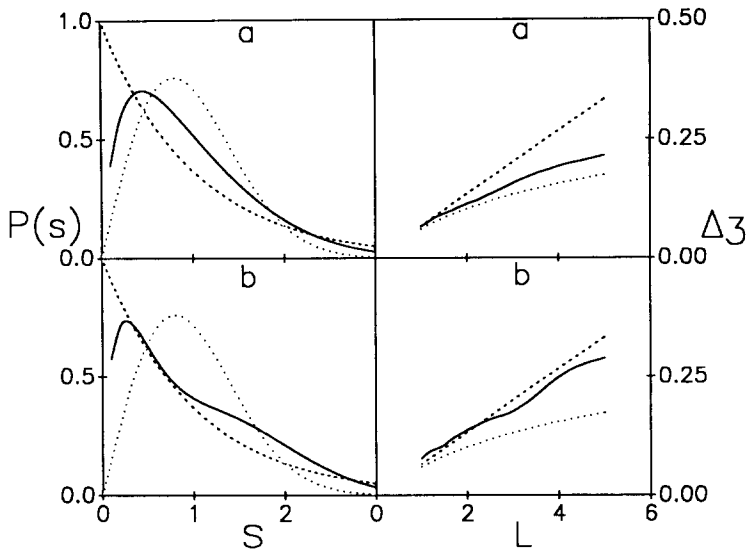

Fig. 4. $P(s)$ and Δ_3 distributions (solid lines) for levels with $m = 0$ (top) and $m = 6$ (bottom). Both the level sequences are of even parity states in a deformed cavity with $\alpha_2 = 0.2$. The ideal Poisson (dashed line) and ideal Wigner (dotted line) distributions are also shown.

of higher order deformations is rather complex and we did not attempt to find the shortest among them for the different systems under consideration. However, we made an estimate of the L_{max} for each system using its typical dimension (assuming the length of the shortest orbit is of the same order) and the average density of energy eigenvalues. In this context, it may be mentioned that the length of the relevant classical orbit is half the length of a fully closed orbit for systems with good parity states [14], e.g. for cavities with even Legendre polynomial deformations. In all other cases, the full length of the periodic orbit is used. The estimated values of L_{max} thus obtained lie in the range of 20–30 and are not marked in the subsequent figures.

We shall now consider cavities described by higher order Legendre polynomials, namely, P_3, P_4, P_5 and P_6. The $P(s)$ and Δ_3 distributions for P_3 and P_4 deformations are given in Figs. 5 and 6, respectively. Both the distributions show Poisson to GOE transitions reaching the full GOE limit for a value of 0.2 of the deformation parameters. Subsequently for P_5 and P_6 deformations, the $P(s)$ and Δ_3 distributions become fully GOE at a value of 0.07 of the deformation parameters, as shown in Figs. 7 and 8, respectively.

3.2. *Systematics of the chaos parameter*

For quantitative discussions, it is often useful to introduce a measure for the degree of chaos for systems that are intermediate between the fully regular and the fully grown chaotic limits. The relative volume of the phase space that belongs to the chaotic trajectories is such a measure for classical systems. For quantum systems, it was shown [15]

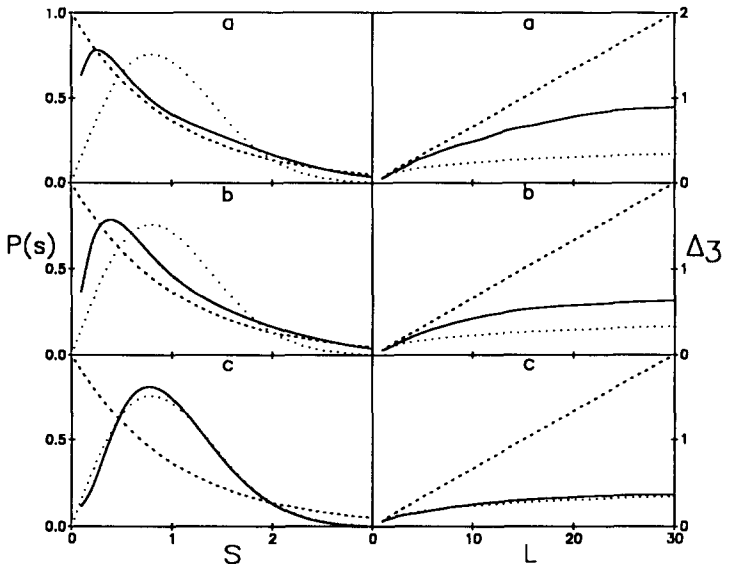

Fig. 5. The nearest neighbor level-spacing distribution $P(s)$ and the spectral rigidity Δ_3 in a P_3 deformed cavity for increasing values of the deformation parameter α_3 starting from the top. The solid lines are the calculated distributions. The ideal Poisson (dashed line) and ideal Wigner (dotted line) distributions are also shown. The figures marked (a), (b) and (c) are for $\alpha_3 = 0.03$, 0.09 and 0.2, respectively. The level sequences are of $m = 0$ states.

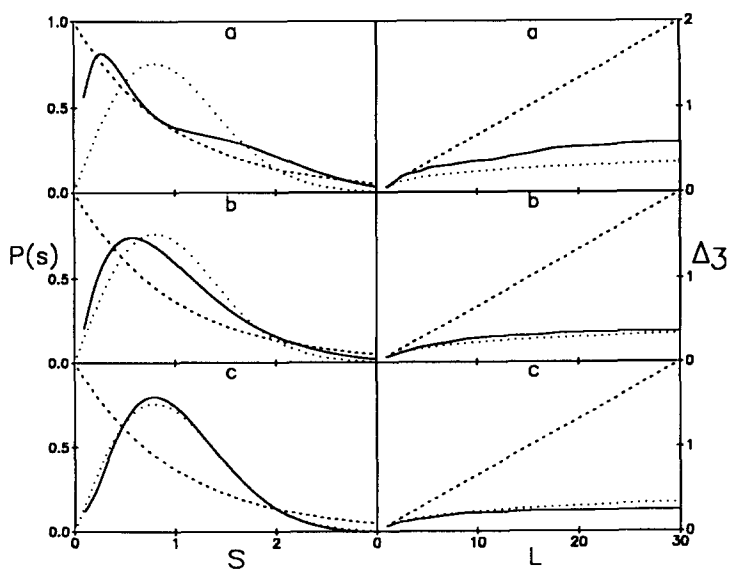

Fig. 6. Same as Fig. 5, but for P_4 deformed cavities. The figures marked (a), (b) and (c) are for $\alpha_4 = 0.03$, 0.09 and 0.2, respectively. The level sequences are of $m = 0$ and even parity states.

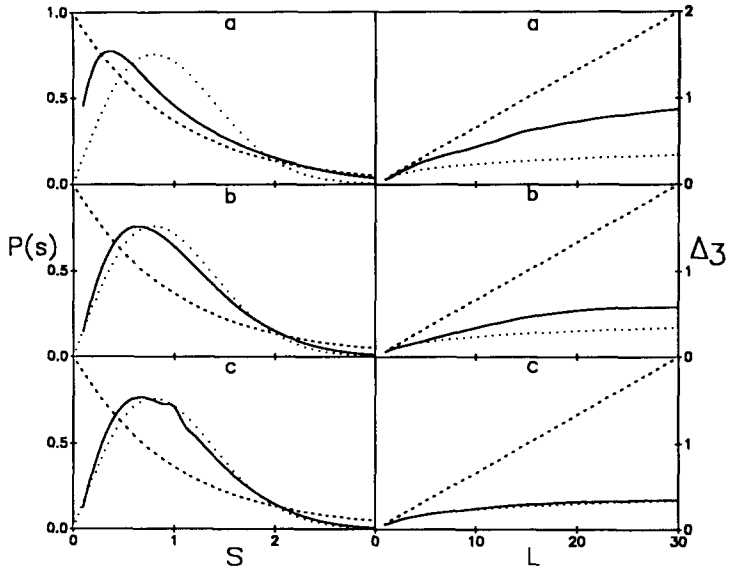

Fig. 7. Same as Fig. 5, but for P_5 deformed cavities. The figures marked (a), (b) and (c) are for $\alpha_5 = 0.01$, 0.05 and 0.07, respectively. The level sequences are of $m = 0$ states.

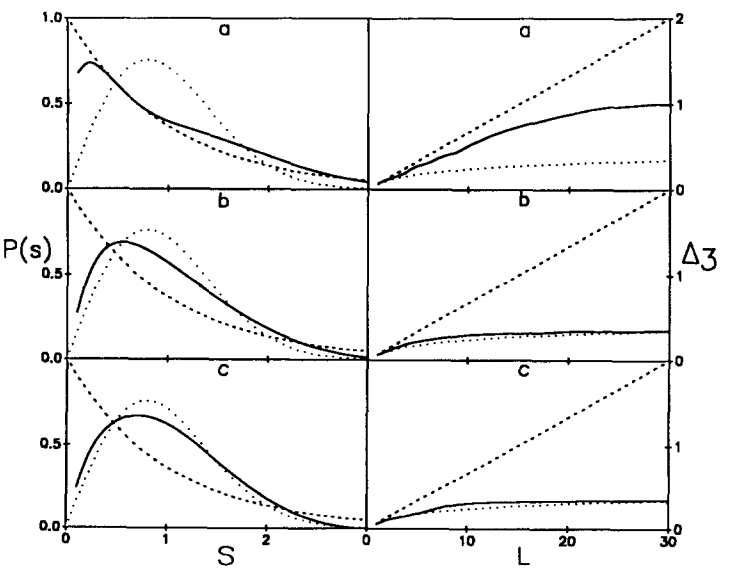

Fig. 8. Same as Fig. 5, but for P_6 deformed cavities. The figures marked (a), (b) and (c) are for $\alpha_6 = 0.01$, 0.05 and 0.07, respectively. The level sequences are of $m = 0$ and even parity states.

semiclassically that the spectra should consist of regular and irregular parts that are associated with the regular and irregular regions in the classical phase space. Subsequently, Berry and Robnik [16] obtained a formula for $P(s)$ by superposing statistically independent Poisson and Wigner sequences of weight factors $(1-\mu)$ and μ respectively, the simplest form of which is given by

$$P_{B-R}(\mu,s) = (1-\mu)^2 e^{-(1-\mu)s}\mathrm{erfc}(\sqrt{\pi}\mu s/2) + [2\mu(1-\mu)+\pi\mu^3 s/2]e^{-[(1-\mu)s+\pi\mu^2 s^2/4]} \tag{3.9}$$

and which smoothly interpolates between Poisson ($\mu = 0$) and Wigner ($\mu = 1$) distributions. For the spectral rigidity, the corresponding distribution is given [17] by

$$\Delta_3(L;\mu) = \Delta_3^P[L(1-\mu)] + \Delta_3^G(L\mu)\,, \tag{3.10}$$

where the superscripts P and G refer to the Poisson and GOE expressions, respectively. Thus for a given spectra, μ can be obtained by fitting the $P(s)$ and Δ_3 distributions and can be used as a measure of irregularity in the system. We shall term μ as the "chaos parameter". Therefore, to study the order-to-chaos transitions in a more quantitative manner, we made a least-square fit of the calculated $P(s)$ and Δ_3 distributions with Eqs. (3.9) and (3.10). The spectral rigidity Δ_3 is fitted in the range $L = 1$–15, which is well within the universal range ($L \ll L_{\max}$) for all the cases.

However, it has been pointed out recently [18] that the Berry–Robnik distribution converges extremely slowly to the semiclassical limit. It was also noted earlier [19] that for near integrable systems, this slow convergence can lead to an overestimation of the chaos parameter. It was further shown [18] that the phenomenological Brody distribution

$$P_{\mathrm{Brody}}(\mu,s) = as^{\mu}e^{-bs^{\mu+1}} \tag{3.11}$$

with $a = (\mu+1)b$ and $b = [\Gamma(1+1/(1+\mu))]^{1+\mu}$ is more appropriate in the near semiclassical regime. Since the number of levels used in the present calculation is not very large (typically 500), we also essentially explore the near semiclassical regime of the single particle dynamics. Subsequently we fitted the $P(s)$ distributions with the above Brody distribution and obtained the chaos parameter. Fig. 9 shows the quality of fit for two typical cases.

The variation of the Berry–Robnik chaos parameter for a cavity with quadrupole deformation when it changes from an oblate to a prolate shape is shown in Fig. 10. For each given deformation, chaos parameters are obtained by separately fitting $P(s)$ and Δ_3 distributions for each parity sequence. The parameters from odd and even parity sequences are very close and the average values are used in this figure. Fig. 10 also shows good agreement between chaos parameters obtained from fitting of the $P(s)$ and the Δ_3 distributions.

The Brody parameter for the P_2 deformed cavity is also shown in Fig. 10 for different deformations. It is immediately seen that though the nature of variation of both the Brody and Berry–Robnik parameters are same, the magnitude of the Brody parameters

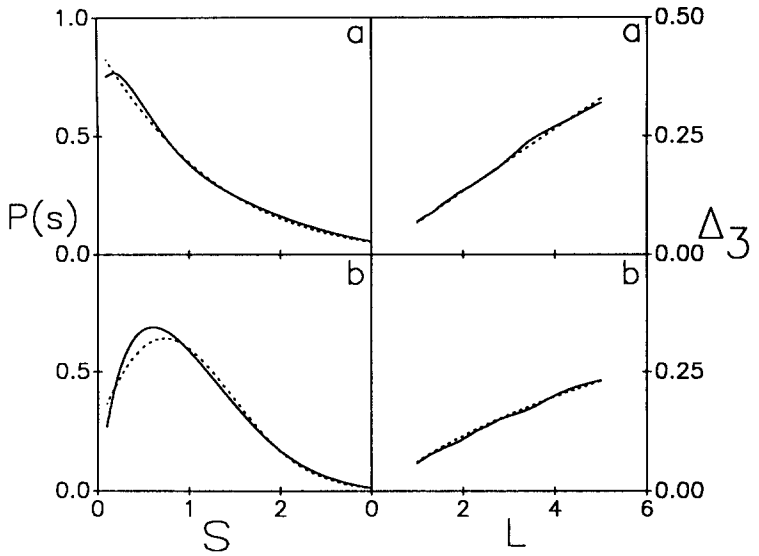

Fig. 9. Typical fits to the calculated (solid lines) $P(s)$ and Δ_3 distributions. The Δ_3 is fitted with Eq. (3.10) and the $P(s)$ with Eq. (3.11), the Brody distribution. The dashed lines are the fitted distributions. The upper and lower figures are for $\alpha_2 = 0.0$ and 0.4 respectively of a P_2 deformed cavity. The level sequences are of $m = 0$ and even parity.

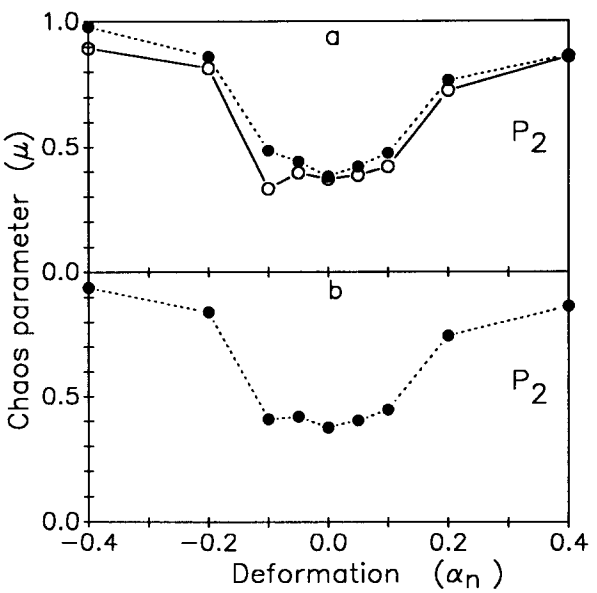

Fig. 10. The chaos parameter μ for different values of the deformation parameter α_n for a cavity with quadrupole deformation ($n = 2$). The plotted values of the chaos parameter are the averages from fitting distributions of even and odd parity sequences. The filled circles (•) are from fitting Δ_3 distributions while the open circles (○) are from fitting $P(s)$ with the Berry–Robnik distribution. The triangles (Δ) are the fitted values using the Brody distribution. The lines joining the points are to guide the eye.

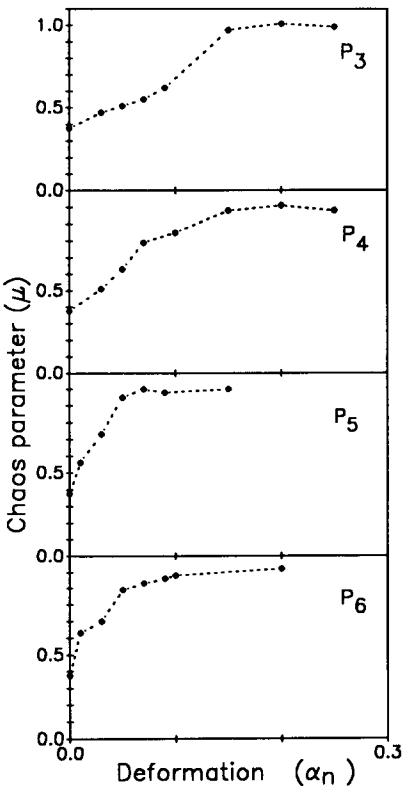

Fig. 11. The chaos parameter μ as a function of the deformation α_n for cavities deformed according to various P_n. The symbols have the same meaning as in Fig. 10. The lines joining the points are to guide the eye.

are much smaller than the Berry–Robnik parameters. In particular, the Brody parameters are much closer to zero for cavities with very small deformations. We find this to be in agreement with the degree of chaos found in the corresponding classical system [4]. We would, therefore, consider the Brody parameter as the appropriate measure of the degree of chaos for the present investigation.

Starting with a small value for the spherical shape, the Brody parameter increases with quadrupole deformation for both the prolate and oblate shapes. However, fully developed chaos ($\mu = 1$) is not reached even at $|\alpha_2| = 0.4$ as was also noted qualitatively in the $P(s)$ and Δ_3 distributions in the earlier sub-section. Fig. 10 further shows the effect of higher asymmetry in oblate shapes giving rise to a higher chaos parameter compared to the corresponding prolate shape with the same value of $|\alpha_2|$.

The variation of the chaos parameter for cavities with higher order polynomial deformations is shown in Fig. 11. Both the Brody and Berry–Robnik parameters are shown in all the plots in this figure, essentially to demonstrate the inadequacy of the Berry–Robnik distribution for systems in the near semiclassical regime. It is also interesting to note that the effect of slow convergence is more pronounced for systems with small deformations than for highly deformed systems where the Brody and Berry–Robnik parameters

converge. We have considered deformations with only positive values in Fig. 11. It is observed in this figure that chaos develops fully in P_3 and P_4 deformed cavities after the deformation parameters reach a value of 0.2 whereas for P_5 and P_6 deformations, chaotic limit is reached even before α_n values of 0.1.

We shall now proceed to obtain the degree of chaos in the single particle motion in deformed cavities which represent nuclear shapes encountered in giant multipole resonances of the nuclei. In a simple macroscopic model, isoscalar giant multipole resonances have been successfully described [8] earlier as harmonic shape oscillations where the stiffness constant is determined from the distortion of the Fermi surface and the inertia is that for an incompressible, irrotational flow of the nucleons. It is easy to see that the amplitude of the deformation in such oscillations for different multipolarities for the lowest mode of excitation lies in the range of 0.05–0.10 for the mass range of $A = 50$ to 200. In Fig. 11 we observe that the chaos parameter for the quadrupole shape varies from 0.1 to 0.2 for $\alpha_2 = 0.05$–0.10 while the chaos parameter for the octupole and hexadecapole shapes for the same values of the deformation parameters falls within 0.2 to 0.4 and 0.3 to 0.6, respectively. For the above range of deformations, the chaos parameter for both the P_5 and P_6 deformed cavities turns out to be within 0.8 to 0.9. We therefore conclude that the chaos in the single particle motion increases with the multipolarity for shapes relevant to the giant resonances in nuclei.

4. Summary and discussions

In the above sections, we have explored the fluctuation properties of the single particle energy spectra in different shaped cavities. Specifically, we considered axially symmetric cavities with deformations following Legendre polynomials of orders from 2 to 6. The fluctuation measures, namely the nearest neighbor level-spacing distribution and the spectral rigidity, displayed a systematic variation with the deformation parameter portraying a transition from order to chaos in the underlying classical motion. The nature of single particle dynamics in Legendre-deformed cavities emerging from the present study of fluctuation measures of quantum energy spectra agreed with that obtained earlier from studies of classical phase space.

We have also studied the variation of the chaos parameter with increasing cavity deformation. The degree of chaos in the single particle dynamics was found to increase with the multipolarity of the cavity deformations which are relevant for the isoscalar giant resonances in nuclei.

Such studies are expected to provide a better understanding of the damping mechanisms of the oscillations of the nuclear surface which are found in the isoscalar multipole giant resonances. Since it is already known [4] that the damping of the shape oscillation of a cavity containing independent particles depends on the non-integrability of the system, it should, therefore, be possible to connect the damping width of the shape oscillation with the degree of chaos in the microscopic dynamics of the system. This aspect is presently under investigation and the results will be reported in a future publication.

Acknowledgements

The authors wish to acknowledge many useful suggestions from Prof. S.C. Phatak, Institute of Physics, Bhubaneshwar regarding numerical solution of the Schrödinger equation.

References

[1] M. Baranger, Proc. Int. Nucl. Phys. Conf., vol. 2, Sao Paulo (World Scientific, Singapore, 1989) p. 247.
[2] W. Nazarewicz and J. Dobaczewski, Phys. Rev. Lett. 68 (1992) 154.
[3] R. Arvieu, F. Brut, J. Carbonell and J. Touchard, Phys. Rev. A 35 (1987) 2389.
[4] J. Blocki, J.-J. Shi and W.J. Swiatecki, Nucl. Phys. A 554 (1993) 387.
[5] J. Blocki, F. Brut, T. Srokowski and W.J. Swiatecki, Nucl. Phys. A 545 (1992) 511c.
[6] W.D. Heiss, R.G. Nazimitdinov and S. Radu, Phys. Rev. Lett. 72 (1994) 2351.
[7] W. Bauer, D. McGrew, V. Zelevinsky and P. Schuck, Phys. Rev. Lett. 72 (1994) 3771.
[8] J.R. Nix and A.J. Sierk, Phys. Rev. C 21 (1980) 396.
[9] A. Honig and D. Wintgen, Phys. Rev. A 39 (1989) 5642.
[10] M.V. Berry and M. Tabor, Proc. R. Soc. London A 356 (1977) 375.
[11] O. Bohigas, M.J. Giannoni and C. Schmit, Phys. Rev. Lett. 52 (1984) 1.
[12] M.V. Berry, Proc. R. Soc. London A 400 (1985) 229.
[13] J.H. Hannay and A.M. Ozorio de Almeida, J. Phys. A 17 (1984) 3429.
[14] Martin C. Gutzwiller, Chaos in classical and quantum mechanics (Springer, Berlin, 1990) p. 312.
[15] I.C. Percival, J. Phys. B 6 (1973) L229.
[16] M.V. Berry and M.J. Robnik, J. Phys. A 17 (1984) 2414.
[17] T.H. Seligman and J.J.M. Verbaarschot, J. Phys. A 18 (1985) 2227.
[18] T. Prosen and M.B. Robnik, J. Phys. A 26 (1993) 2371.
[19] Th. Zimmermann, H.D. Meyer, H. Koppel and L.S. Cederbaum, Phys. Rev. A 33 (1986) 4334.